

*Electronic Supplementary Information (ESI)*

## **Tuning amounts of redox groups in cathode toward high rate and long lifespan zinc-ion batteries**

YanJun Shi,<sup>a, \*</sup> Zhihui Xu,<sup>a</sup> Pengcheng Wang,<sup>a</sup> Haiguang Gao,<sup>a</sup> Wanjiao He,<sup>a</sup> Yanan Sun,<sup>b</sup> Yucheng Huang,<sup>c</sup> Juan Xu,<sup>a</sup> and Jianyu Cao<sup>a, \*</sup>

<sup>a</sup> *Jiangsu Key Laboratory of Advanced Catalytic Materials and Technology, Analysis and Testing Center, School of Petrochemical Engineering, Changzhou University, 1 Gehu Road, Changzhou, Jiangsu 213164, China.*

<sup>b</sup> *Beijing National Laboratory for molecular Sciences, Key Laboratory of Organic Solids, Institute of Chemistry, Chinese Academy of Sciences, Beijing 100190, China.*

<sup>c</sup> *College of Chemistry and Material Science, Anhui Normal University, Wuhu 241000, China.*

\*Corresponding author. E-mail: [shianjun@cczu.edu.cn](mailto:shianjun@cczu.edu.cn) (Y. Shi); [jycao@cczu.edu.cn](mailto:jycao@cczu.edu.cn) (J. Cao).

## Experimental section

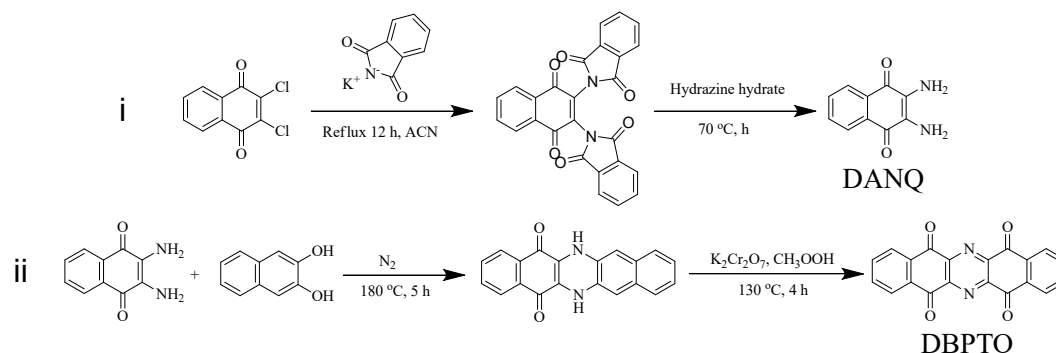
### Materials

All the raw materials and reagents were commercially purchased and used as received without further purification.

### Characterization

The liquid state  $^1\text{H}$  and solid state  $^{13}\text{C}$  nuclear magnetic resonance (NMR) spectra were measured on the Bruker AVANCE III HD 400 MHz spectrometer and Bruker AVANCE III 400 MHz spectrometer, respectively. High resolution mass spectra (HRMS) were recorded on Alliance e2695 spectrometer. Fourier transform infrared (FT-IR) spectroscopy were recorded on a Nicolet iN10 spectrometer instrument using a KBr pellet. Scanning electron microscopy (SEM) images were carried out on a JSM 6360LA instrument. X-ray diffraction (XRD) measurements were performed on a Rigaku D/max2500 instrument with Cu K $\alpha$  radiation. Thermogravimetric analysis (TGA) was carried out on a Simultaneous Thermal Analyzer 6000 at a heating rate of  $10\text{ }^\circ\text{C min}^{-1}$  under a nitrogen flow of  $40\text{ mL min}^{-1}$ . The oxidation states of materials were analyzed by X-ray photoelectron spectroscopy (Thermo Scientific K-Alpha XPS System).

### Synthesis of dibenzo[b,i]phenazine-5,7,12,14-tetraone (DBPTO)



**Scheme S1.** Synthetic route of DBPTO

i. 2,3-diamino-1,4-naphthoquinone (DANQ) was synthesized according to the previous report.<sup>1</sup> 10 g 2,3-dichloro-1,4-naphthoquinone (DCNQ, Energy Chemical, 98%) was dissolved in 150 mL anhydrous acetonitrile (ACN) and 20 g potassium phthalimide (Energy Chemical, 98%) was added. The mixture was stirred and refluxed for 12 h in nitrogen atmosphere. The yellow solids were filtered and dried under vacuum. The solid was dispersed in 150 mL hydrazine hydrate and stirred at 70°C for 12 h. After cooling to room temperature, the modena powder was filtered and washed with water to afford DANQ. <sup>1</sup>H-NMR (400M, DMSO-*d*<sub>6</sub>) δ (ppm) 5.46 (s, 4H), 7.57-7.61 (m, 2H), 7.73-7.78 (m, 2H).

ii. DBPTO was synthesized by a modified method according to the previous reports. Firstly, 1.6 g 2,3-dihydroxynaphthalene and 1.9 g DANQ were mixed thoroughly using a pestle and mortar. Then the mixture was heated with stirring at 180 °C for 5 h under nitrogen flow. After cooling to room temperature, the mixture was filtered and washed several times with deionized water and acetone successively, and then dried at 80 °C in vacuum for 18 h to obtain a black powder of dibenzo[*b,i*]phenazine-5,14(6H,13H)-dione (DBPDO). Secondly, 0.2 g DBPDO was dissolved in 15 mL glacial acetic acid, then 1.5 g K<sub>2</sub>CrO<sub>7</sub> was added as an oxidant. The mixture was heated at 130 °C for 4 h. After cooling to room temperature, the suspension was then filtered, washed with deionized water and acetone subsequently, and dried at 80 °C in vacuum for 18 h to finally obtain the DBPTO brown power. <sup>1</sup>H-NMR (400 MHz, DMSO-*d*<sub>6</sub>): δ (ppm) 5.46 (s, 4H), 8.02-8.05 (m, 2H), 8.33-8.36 (m, 2H); <sup>13</sup>C NMR (400 MHz) δ (ppm) 180.3, 142.8, 137.4, 133.2, 128.9.

## **Electrochemical measurements**

The aqueous zinc-ion batteries (CR2032) were composed of organic cathode, zinc foil, separator, and 2 M ZnSO<sub>4</sub> aqueous solution. The organic cathode was prepared by mixing DBPTO, Ketjen black ECP600JD (KB) and polytetrafluoroethylene (PVDF) with a mass ratio of 6:3:1, and then the obtained slurry was coated onto a carbon paper (diameter = 14 mm) and dried in vacuum at 110 °C for 24 h. The mass loading of active materials in the electrode is about 0.5-1.0 mg cm<sup>-2</sup>. The metallic zinc foil was used as anodes with a diameter of 16 mm and a thickness of 0.15-0.25 mm, respectively. The glass fiber membrane (GF/D, diameter = 19 mm) was used as a separator.

Cyclic voltammetry (CV) tests were carried out using a CHI 660E electrochemical workstation. The discharge-charge curves, rate performance, and cycling stability of the aqueous Zn//DBPTO batteries were estimated using a Shenzhen Neware battery testing system. The cycling performance was tested under 0.05 A g<sup>-1</sup> at first 15 cycles.

## **Density functional theory computation**

The neutral ground state molecular structure optimization and frontal orbital distribution were obtained by density functional theory (DFT) at the B3LYP/6-31G\* and PW91PW91/6-31G\* level, which were carried out using the Gaussian 16 program package. The electronic structure calculations was realized using the VASP 5.4.4 software package<sup>2</sup> by the projector-augmented wave (PAW) method<sup>3</sup> with generalized gradient approximation (GGA) within Perdew–Burke–Ernzerhof (PBE)<sup>4,5</sup>. The cutoff of 400 eV was used during the calculation. The energy and force

convergence criteria were set to  $10^{-5}$  eV and  $5 \times 10^{-2}$  eV  $\text{\AA}^{-1}$ , respectively. The water was considered as solvent using the VASP<sub>sol</sub> package.

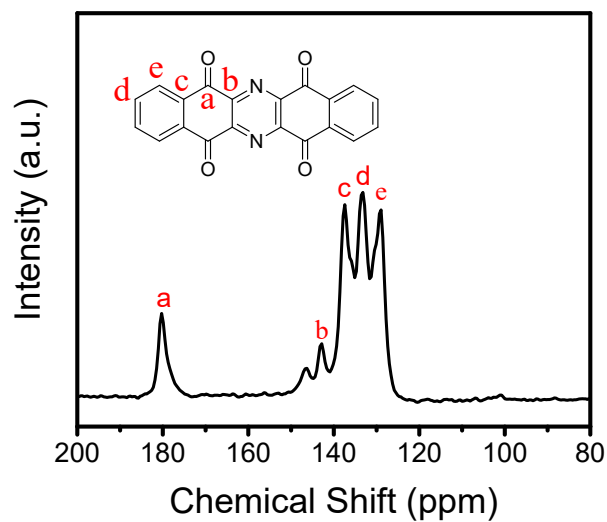


Fig. S1  $^{13}\text{C}$  NMR spectrum of DBPTO.

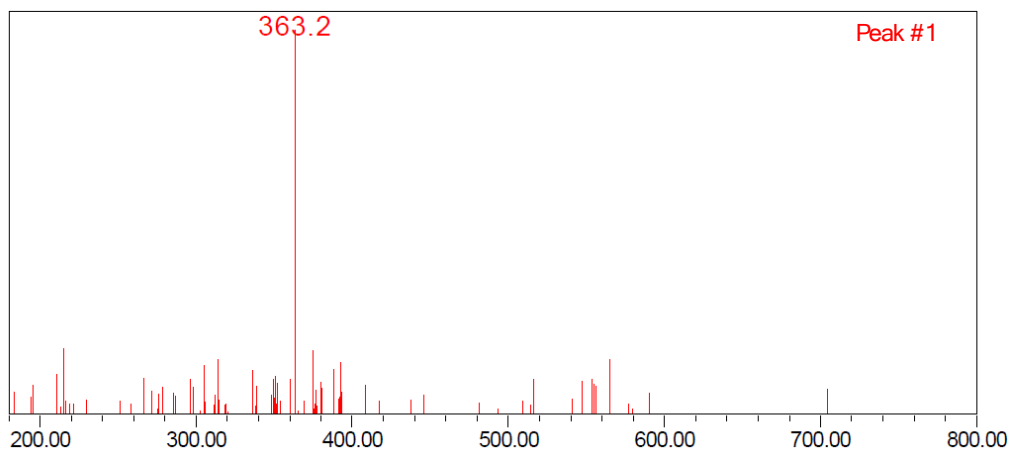


Fig. S2 HRMS of DBPTO. Calculated for  $[\text{DBPTO}+\text{Na}]^+$ : 363.29, found:363.2.

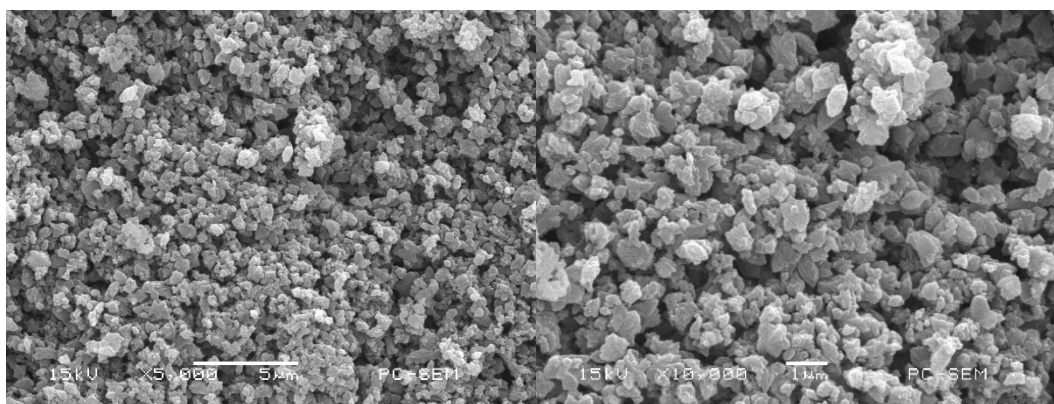


Fig. S3 SEM images of DBPTO.

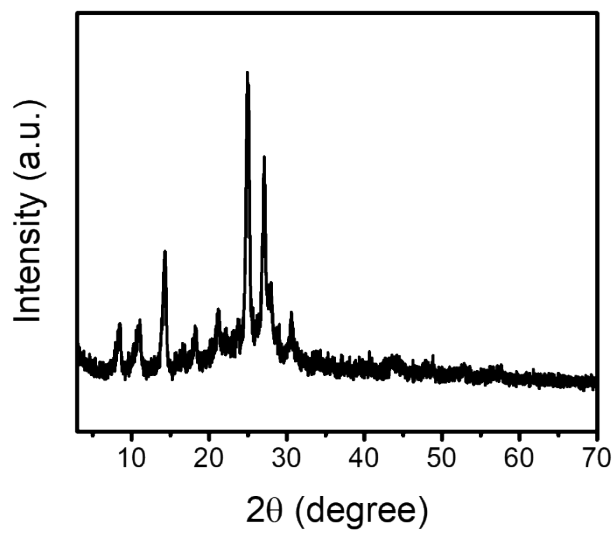


Fig. S4 XRD pattern of DBPTO.

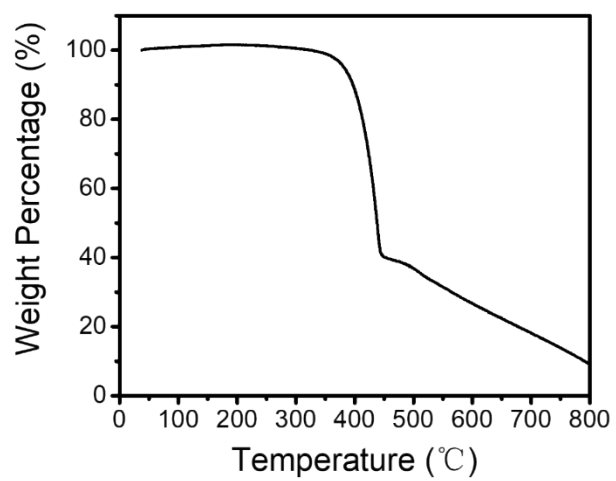


Fig. S5 TGA result of DBPTO.

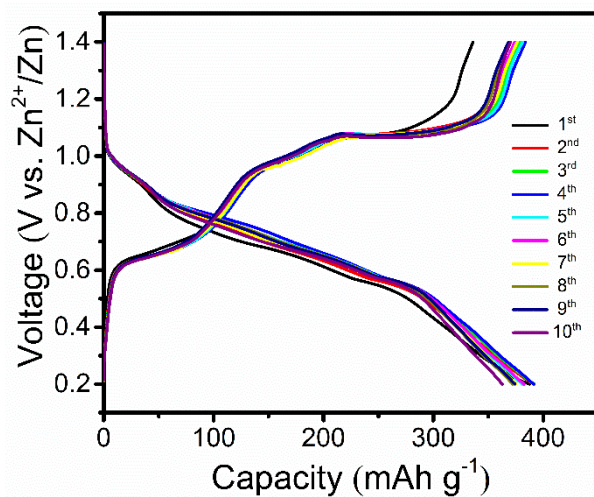


Fig. S6 The discharge-charge profiles at 0.05 A g<sup>-1</sup> of DBPTO.

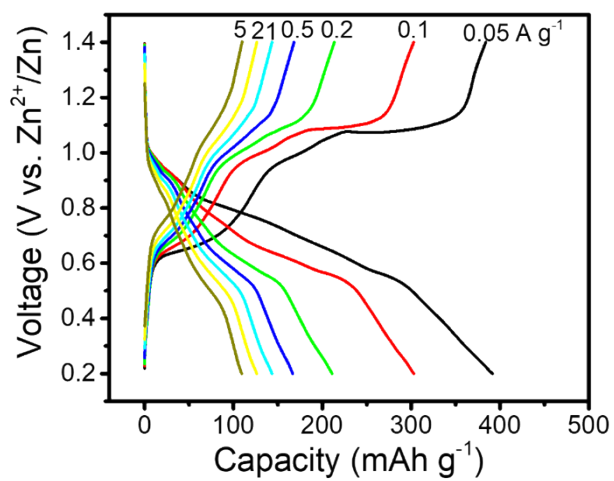


Fig. S7 The discharge-charge profiles under different current densities of DBPTO.



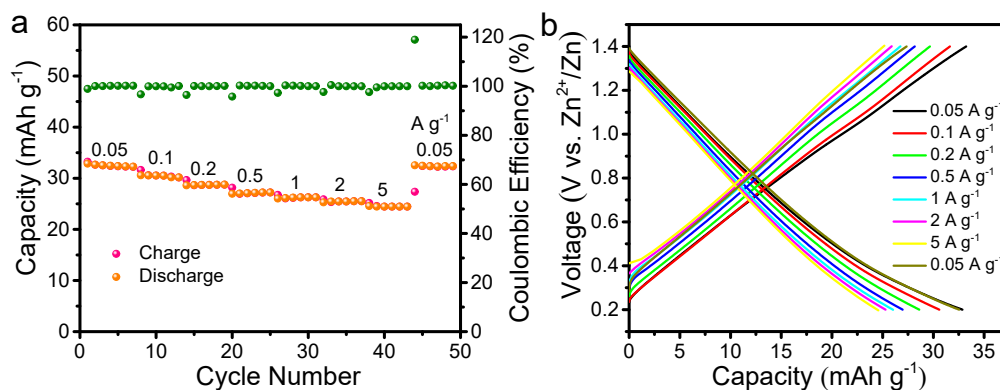


Fig. S8 Electrochemical performance of the conductive additive (KB). (a) Typical discharge/charge curves, and (b) the capacity at different current densities in the range of 0.2-1.4 V.

The KB electrodes were obtained by mixing KB and PVDF with a mass ratio of 9:1.

Since the DBPTO electrode is composed of DBPTO: KB: PVDF = 6:3:1, the contribution of KB to the DBPTO electrode is  $0.5C_{KB}$ , and the formula is as follows:

$$C = (6 \times C_{DBPTO} + 3 \times C_{KB}) / 6 = C_{DBPTO} + 0.5C_{KB}$$

Where, C is the apparent specific capacity only based on the DBPTO,  $C_{DBPTO}$  is the actual specific capacity of DBPTO, and the  $C_{KB}$  is the measured specific capacity of KB.

Here, the value of  $C_{KB}$  is 32.87-24.57  $\text{mAh g}^{-1}$ . So, the capacity contribution of KB is about 16.43-12.29  $\text{mAh g}^{-1}$ , which is negligible for the capacity of  $C_{DBPTO}$ .

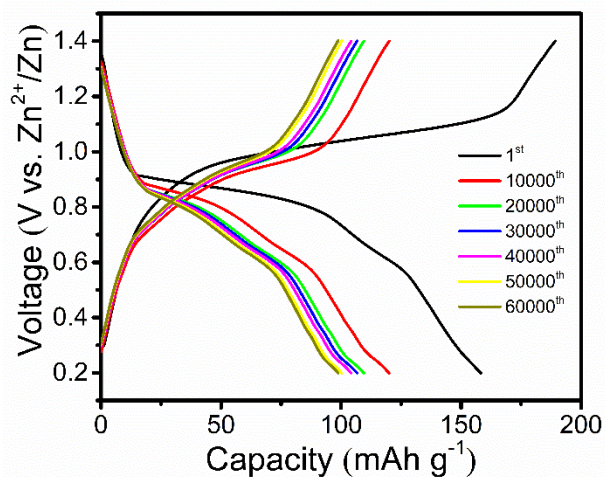


Fig. S9 The discharge-charge profiles at 5 A g<sup>-1</sup> of DBPTO.

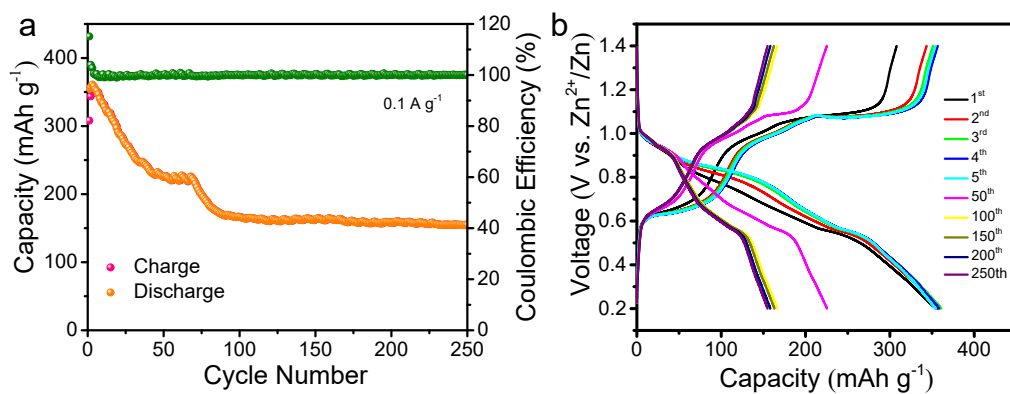
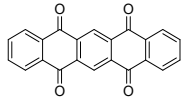
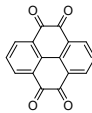
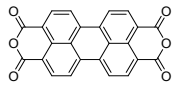
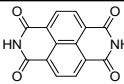
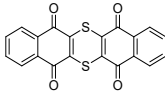
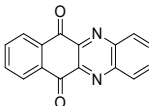
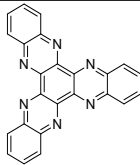
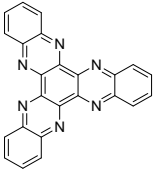
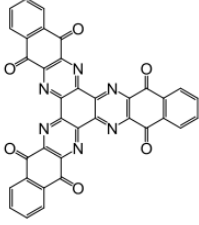
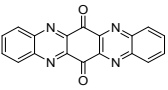
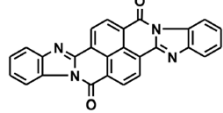
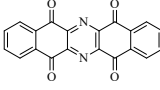


Fig. S10 (a) Cycling performance and (b) corresponding discharge-charge profiles at 0.1 A g<sup>-1</sup> of DBPTO.

**Table S1.** The comparison of electrochemical performances of DBPTO with previously reported small molecule organic cathodes in aqueous zinc-ion batteries. (<sup>a</sup> The capacity retention is the ratio of the discharge capacity of the final cycle to the maximum discharge capacity.)

Cathode Materials	Electrolyte	Theoretical specific capacity (mAh g <sup>-1</sup> ), Electron transfer number	Reversible capacity (mAh g <sup>-1</sup> , A g <sup>-1</sup> )	Capacity at last cycle, capacity retention <sup>a</sup> (A g <sup>-1</sup> , cycle number)	Refs.
 PT	2 M ZnSO <sub>4</sub>	317 4	(220, 0.08) (100, 20)	127, 95% (2.5, 5 000)	6
 PTO	2 M ZnSO <sub>4</sub>	409 4	(336, 0.04) (110, 20)	145, 63% (3, 1 000)	7
 PTCDA	2 M ZnCl <sub>2</sub>	273 4	(122.9, 0.2) (98, 8)	67, 68% (8, 1 000)	8
 NTCDI	2 M ZnSO <sub>4</sub>	403 4	(240, 0.1) (130, 2)	112, 72% (1, 2 000)	9
 DTT	2 M ZnSO <sub>4</sub>	285 4	(211, 0.05) (97, 2)	80, 74% (2, 23 000)	10
 BPD	2 M ZnSO <sub>4</sub>	412 4	(429, 0.05) (135, 5)	99, 73% (5, 10 000)	11
 DQP	1 M ZnSO <sub>4</sub>	418 6	(413, 0.05) (188, 5)	162, 70% (5, 1 000)	12

 <p><b>HATN</b></p>	2 M ZnSO <sub>4</sub>	418 6	(370, 0.1) (150.5, 5)	140, 90% (5, 5 000)	13
 <p><b>HATNQ</b></p>	2 M ZnSO <sub>4</sub>	510 12	(455.7, 0.2) (177.5, 9)	200, 73% (5, 11 000)	14
 <p><b>TAPQ</b></p>	1 M ZnSO <sub>4</sub>	515 6	(443, 0.05) (~25, 5) (270, 0.05) (81, 5)	248, 56% (0.05, 100) 65, 26% (0.5, 2 000)	15
 <p><b>BBPD</b></p>	2 M ZnSO <sub>4</sub>	260 4	(127, 0.1) (97, 20)	88, 90.7% (20, 10 000)	16
 <p><b>DBPTO</b></p>	2 M ZnSO <sub>4</sub>	472 6	(380, 0.05) (108, 5)	98, 62% (5, 60 000)	This work

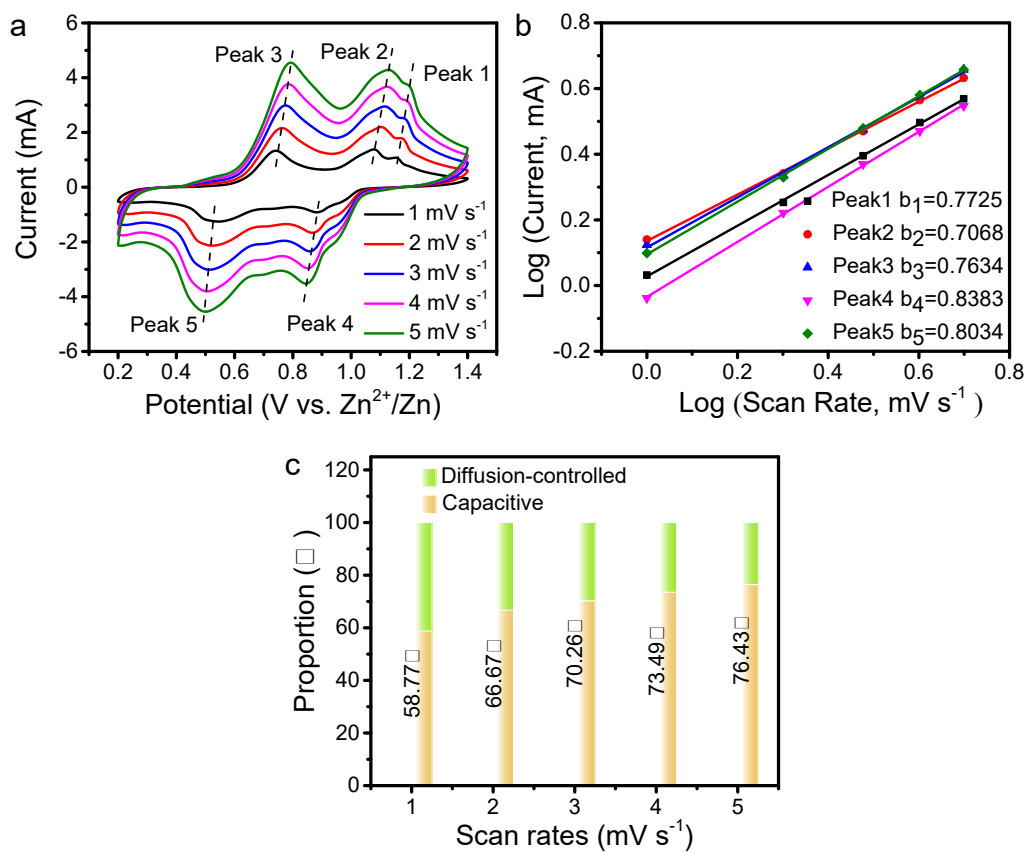


Fig. S11 (a) CV curves of DBPTO at different scan rates from 1 to 5 mV s<sup>-1</sup>. (b) The fitted plots between log (scan rate) and log (peak current). (c) Capacity contribution ratio at different scan rates.

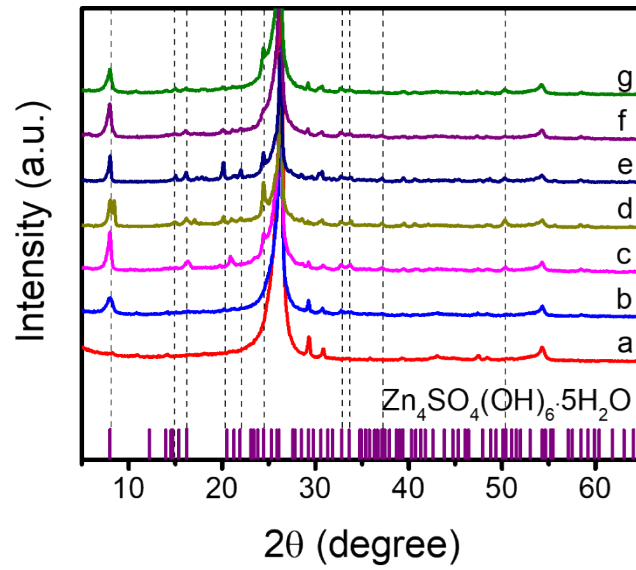


Fig. S12 XRD patterns at selected states in Fig. 3(a) of the DBPTO electrode.

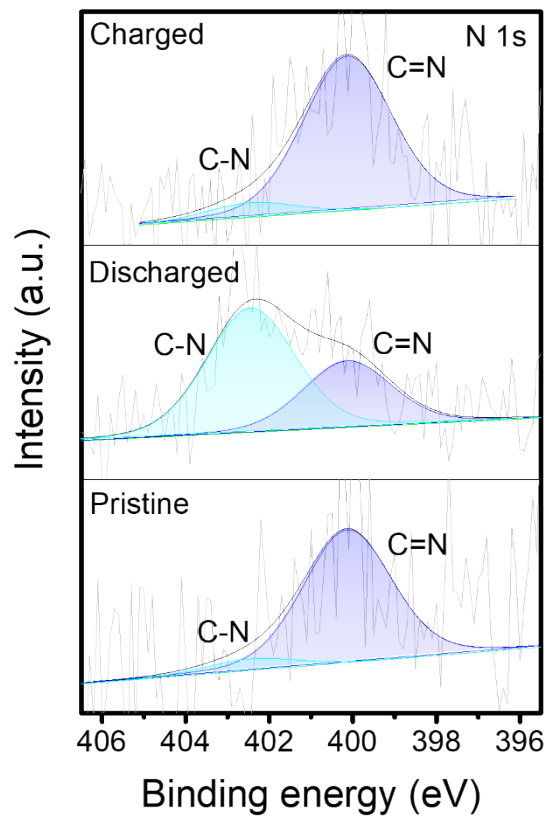


Fig. S13 N 1s XPS spectra (C-N and C=N are located at 402.44 and 400.13 eV) at pristine, fully discharge and charged states of DBPTO electrode.

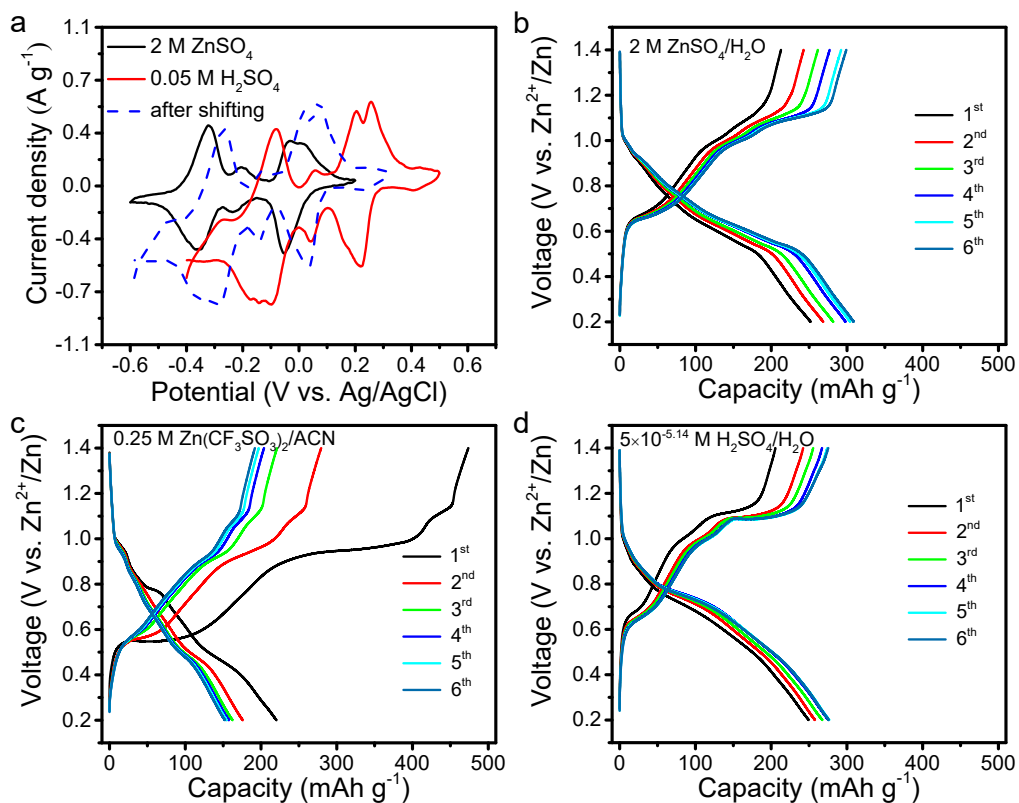


Fig. S14 (a) CV curves of DBPTO at  $0.2 \text{ mV s}^{-1}$  in  $2 \text{ M ZnSO}_4$  and  $0.05 \text{ M H}_2\text{SO}_4$  aqueous electrolyte. The dotted line is the corresponding CV curves in  $0.05 \text{ M H}_2\text{SO}_4$  after being shifted according to Nernst equation. Discharge/charge voltage profiles at  $0.1 \text{ A g}^{-1}$  of DBPTO in (b)  $2 \text{ M ZnSO}_4$ , (c)  $0.25 \text{ M Zn}(\text{CF}_3\text{SO}_3)_2/\text{CAN}$ , and (d)  $5 \times 10^{-5.14} \text{ M H}_2\text{SO}_4$  electrolyte.

## References

1. G. Xie, M. Hauschild, H. Hoffmann, L. Ahrens, F. Rominger, M. Borkowski, T. Marszalek, J. Freudenberg, M. Kivala and U. H. F. Bunz, *Chem. Eur. J.*, 2020, 26, 799.
2. G. Kresse and D. Joubert. *Phys. Rev. B*, 1999, 59, 1758.
3. P.E. Blochl. *Phys. Rev. B*, 1994, 50, 17953.
4. J.P. Perdew, K. Burke and M. Ernzerhof. *Phys. Rev. Lett.* 1996, 77, 3865.
5. K. Mathew, V.S.C. Kolluru, S. Mula, S.N. Steinmann and R.G. Hennig. *J. Chem. Phys.* 2019, 151, 234101.
6. C. Mirle, V. Medabalmi and K. Ramanujam. *ACS Appl. Energy Mater.* 2021, 4, 1218.
7. Z. Guo, Y. Ma, X. Dong, J. Huang, Y. Wang and Y. Xia. *Angew. Chem. Int. Ed.* 2018, 57, 11737.
8. H. Zhang, Y. Fang, F. Yang, X. Liu and X. Lu. *Energy Environ. Sci.* 2020, 13, 2515.
9. X. Wang, L. Chen, F. Lu, J. Liu, X. Chen and G. Shao. *ChemElectroChem*, 2019, 6, 3644.
10. Y. Wang, C. Wang, Z. Ni, Y. Gu, B. Wang, Z. Guo, Z. Wang, D. Bin, J. Ma and Y. Wang. *Adv. Mater.* 2020, 32, e2000338.
11. Y. Shi, P. Wang, H. Gao, W. Jin, Y. Chen, Y. Huang, T. R. Wu, D.Y. Wu, J. Xu and J. Cao. *Chem. Eng. J.* 2023, 461, 141850.
12. H. Zhang, S. Xie, Z. Cao, D. Xu, L. Wang, H. Fang, J. Shen and M. Ye. *ACS Appl. Energy Mater.* 2021, 4, 655.
13. Z. Tie, L. Liu, S. Deng, D. Zhao and Z. Niu. *Angew. Chem. Int. Ed.* 2020, 59, 4920.
14. Y. Chen, J. Li, Q. Zhu, K. Fan, Y. Cao, G. Zhang, C. Zhang, Y. Gao, J. Zou, T. Zhai and C. Wang. *Angew. Chem. Int. Ed.* 2022, 61, e202116289.
15. Y. Gao, G. Li, F. Wang, J. Chu, P. Yu, B. Wang, H. Zhan and Z. Song. *Energy Stor. Mater.*, 2021, 40, 31.
16. Q. Wang, Y. Liu, C. Wang, X. Xu, W. Zhao, Y. Li and H. Dong. *Chem. Eng. J.* 2023, 451, 138776.